Reversal of extreme precipitation trends over the Northeast US in response to aggressive climate mitigation in GFDL SPEAR

Bor-Ting Jong[1,2,3,*], Zachary M. Labe[4,5], Thomas L. Delworth[5], and Willam F. Cooke[5]

[1] Department of Earth Sciences, Vrije Universiteit Amsterdam, Amsterdam, The Netherlands

[2] Institute for Environmental Studies, Vrije Universiteit Amsterdam, Amsterdam, The Netherlands

[3] Atmospheric and Oceanic Sciences Program, Princeton University, Princeton, NJ, USA

[4] Climate Central, Inc., Princeton, NJ, USA

[5] NOAA/OAR/Geophysical Fluid Dynamical Laboratory, Princeton, NJ, USA

*Corresponding author: Bor-Ting Jong (b.jong@vu.nl)

Keywords: extreme precipitation, climate variability, climate change, overshoot, climate mitigation, reversibility, climate impacts, climate models, large ensembles, future scenarios, Northeast US

Submitted to Environmental Research Letters

Abstract

Rapid reductions in greenhouse gas (GHG) concentrations are increasingly included in mitigation strategies, yet the response of regional climate extremes to such reductions remain highly uncertain. Here, we assess projected changes in extreme precipitation over the Northeast US under an aggressive overshoot mitigation pathway (SSP5-3.4OS), simulated by the fully coupled 25-km GFDL SPEAR climate model. In this scenario, hypothetical mitigation efforts are introduced starting in 2041, with net-negative GHG emissions achieved by the late 21st century. The frequency of extreme precipitation over the Northeast US increases through mid-century under higher radiative forcing but begins to decline following the sharp reductions in GHG concentrations. However, the rate of decrease exhibits pronounced seasonality. In the warm season, extreme precipitation frequency begins to decline shortly after GHG drawdown begins, returning by 2100 to levels comparable to those of the early 21st century. In the cold season, on the other hand, the response is delayed; the frequency of extreme precipitation continues rising for roughly a decade after the peak global mean warming and exhibits hysteresis behavior. By 2100, cold-season extremes only then return to mid-century levels. This delayed response in the cold season is spatially heterogeneous, suggesting that major metropolitan areas in the Northeast – with dense populations and vulnerable infrastructure – may experience different seasonal changes in response to the same climate migration efforts. These results highlight the benefit of climate mitigation in reducing extreme precipitation events, but also the complexity of regional climate responses, which can be modulated by seasonality, local-scale effects, and other factors.

1. Introduction

Extreme precipitation has increased over many land areas globally since the mid-20th century (e.g., Westra et al. 2013; Donat et al. 2013, 2016; Asadieh and Krakauer 2015; Dunn et al. 2020; Sun et al. 2021). At least part of this rise has been attributed to anthropogenic forcing (Min et al. 2011; Zhang et al. 2013; Fischer and Knutti 2015, 2016; Seneviratne et al. 2021), and extreme precipitation is projected to continue increasing with greater global warming (Fowler and Hennessy 1995; O'Gorman and Schneider 2009; O'Gorman 2015; Donat et al. 2016; Seneviratne et al. 2021; Thackeray et al. 2022; Kotz et al. 2024). In recent years, new climate scenarios have been developed to begin exploring the effects of rapidly reducing greenhouse gases (GHG) through plausible future climate mitigation pathways. Many of these efforts aim to limit global warming levels to below 1.5°C or 2°C above preindustrial levels – the targets established in the Paris Agreement (Azar et al. 2013; UNFCC 2015; Rogelj et al. 2018; Kikstra et al. 2022; IPCC 2022; Prütz et al. 2023; Schleussner et al. 2024). While the global mean surface temperature (GMST) is expected to decline monotonically in response to falling GHG concentrations (Samanta et al. 2010; Boucher et al. 2012; Tokarska et al. 2019; Tebaldi et al. 2021; Delworth et al. 2022; Koven et al. 2022; Kim et al. 2022; Labe et al. 2024; Pfleiderer et al. 2024), the responses of other aspects of the climate system – especially regional extreme events – remain more uncertain and comparatively understudied (Mondal et al. 2023; Pfleiderer et al. 2024; Reisinger et al. 2025; Roldán-Gómez et al. 2025).

Due to the nonlinear nature of the climate system and the varying timescales of its different components, the responses of climate variables to declining GHG concentrations may not be fully reversible to their initial states (climate reversibility) and/or exhibit lagged, path-dependent behaviors (hysteresis) (Solomon et al. 2009; Held et al. 2010; Boucher et al. 2012; Zickfeld et al. 2013; Tebaldi and Friedlingstein 2013; Mathesius et al. 2015; Samset et al. 2020; Melnikova et al. 2021; Koven et al. 2022; Schleussner et al. 2024; Pfleiderer et al. 2024; Reisinger et al. 2025; Roldán-Gómez et al. 2025). Sea level is one example that is effectively irreversible on timescales relevant to human society, with ocean waters continuing to rise well beyond the point when net-zero GHG emissions are achieved (Ehlert and Zickfeld 2018; Mengel et al. 2018; Palter et al. 2018). On the other hand, other variables, like global mean precipitation, show path dependance and follow distinct trajectories during phases of global warming increase and subsequent decrease (e.g., Cao et al. 2011; Jeltsch-Thömmes et al. 2020; Zickfeld et al. 2021; Kim et al. 2022; Walton and Huntingford 2024). This hysteresis mainly arises from the large inertia and multiple feedback processes within the climate system, thus leading to a delayed recovery in response to decreasing radiative forcing (e.g. Held et al. 2010; Cao et al. 2011; Boucher et al. 2012; An et al. 2021; Zickfeld et al. 2021; Delworth et al. 2022; Koven et al. 2022). In addition, responses to radiative forcing can also be modulated by dynamical processes at local and regional scales (Chadwick et al. 2013; Zappa et al. 2020; Delworth et al. 2022) and/or through internal variability (Tebaldi and Friedlingstein 2013; Deser 2020; Diffenbaugh et al. 2023; Walton and Huntingford 2024).

At this stage, the GMST is highly likely to (at least temporarily) exceed the target warming limits (Huntingford and Lowe 2007; Raftery et al. 2017; Hausfather and Peters 2020; Peters 2024; Forster et al. 2025; Hausfather 2025). Aggressive mitigation efforts with rapid GHG drawdowns are, therefore, more likely to be required (Gasser et al. 2015; Tebaldi et al. 2021; IPCC 2022; Kikstra et al. 2022; Schleussner et al. 2024). To then assess the effects of rapid GHG reductions, an array of studies have used idealized carbon dioxide (CO_2) removal scenarios, in which CO_2 concentrations are linearly ramped up and then symmetrically ramped down (e.g., Samanta et al. 2010; Boucher et al. 2012; Chadwick et al. 2013; Zickfeld et al. 2016; An et al. 2021; Kim et al. 2022; Mondal et al. 2023; Hwang et al. 2024; Steinert et al. 2025). More recently, studies have started using comprehensive climate models or Earth System Models to simulate overshoot scenarios (such as the Shared Socioeconomic Pathway 5-3.4OS, SSP5-3.4OS) (Melnikova et al. 2021, 2023; Delworth et al. 2022; McHugh et al. 2023; Li et al. 2024; Pfleiderer et al. 2024; Roldán-Gómez et al. 2025; Labe et al. 2025). In these overshoot scenarios, global warming level temporarily exceeds 2°C before declining in response to mitigation efforts (O'Neill et al. 2016). Under SSP5-3.4OS, temperature and heat extremes over Northern Hemisphere land areas are generally reversible – albeit with varying degrees of delay – by the end of 21st century (McHugh et al. 2023; Pfleiderer et al. 2024; Roldán-Gómez et al. 2025; Labe et al. 2025). In contrast, the responses of mean and extreme precipitation exhibit greater spatial heterogeneity (Walton and Huntingford 2024; Pfleiderer et al. 2024; Roldán-Gómez et al. 2025) and stronger seasonality (Tebaldi and Friedlingstein 2013; Delworth et al. 2022). For example, Mediterranean rainfall, projected to decline under warming, shows mixed reversibility in SSP5-3.4OS: while summer drying is reversible, winter rainfall continues to decline even after the dramatic GHG drawdowns

(Delworth et al. 2022). This continued winter drying is linked to the prolonged weakening of the Atlantic Meridional Overturning Circulation (AMOC), driven by increased GHGs, and it recovers only slowly. The weakening AMOC induces a persistent anomalous anticyclone that steers winter storms away from the region (Delworth et al. 2022). This example highlights the need for more targeted and region-specific analyses to understand changes in regional precipitation patterns.

In this study, we focus on the changes in extreme precipitation over the Northeast United States (US). The Northeast US has experienced the largest increase in extreme precipitation in the US, particularly since the mid-1990s (e.g., DeGaetano 2009; Brown et al. 2010; Kunkel et al. 2013; Thibeault and Seth 2014; Frei et al. 2015; Guilbert et al. 2015; Hoerling et al. 2016; Huang et al. 2017, 2018; Howarth et al. 2019; DeGaetano et al. 2020; Olafsdottir et al. 2021; Henny et al. 2022, 2023; Crossett et al. 2023; Jong et al. 2023, 2024; Marvel et al. 2023; Whitehead et al. 2023). This trend is evident in all seasons, even though the dominant physical drivers of extreme precipitation vary seasonally (Kunkel et al. 2012; Agel et al. 2015, 2018; Huang et al. 2018; Howarth et al. 2019; Jong et al. 2024). Extreme precipitation over the Northeast US is projected to continue increasing under anthropogenic warming (e.g., Hayhoe et al. 2007; Thibeault and Seth 2014; Ning et al. 2015; DeGaetano and Castellano 2017; Nazarian et al. 2022; Picard et al. 2023; Jong et al. 2023, 2024). This extreme precipitation trend poses growing flood risks for the densely populated Northeast, home to several major metropolitan areas including New York City, Washington D.C., Philadelphia and Boston. With millions of people and critical infrastructure at risk, understanding how extreme precipitation may respond under different climate scenarios is essential for informing urban adaptation and resiliency strategies.

To assess how extreme precipitation in the Northeast US may change in a scenario of aggressive climate mitigation, we leverage simulations from the fully coupled 25-km GFDL (Geophysical Fluid Dynamics Laboratory) SPEAR (**S**eamless system for **P**rediction and **EA**rth system **R**esearch) model, which includes multiple ensemble members and a suite of climate scenarios. The choice of this high-resolution model is motivated by previous studies showing that climate models with finer atmospheric horizontal resolution (e.g., < 50 km) better simulate extreme precipitation, especially at regional scales, than coarser-resolution models (e.g., 100-200km) (Wehner et al. 2010, 2014; Kopparla et al. 2013; Van der Wiel et al. 2016; Schiemann et al. 2018; Iles et al. 2020; Stansfield et al. 2020; Jong et al. 2023). We first examine how extreme precipitation changes with GMST warming level and focus on comparing the warm season (June to November; consistent with the Atlantic hurricane season) and the cold season (December to May) responses, which aim to reflect their distinct dominant precipitation characteristics. We then briefly explore how these responses vary across different urban areas within the Northeast US.

2. Data and method

2.1 Model and simulations

We use a suite of future climate simulations conducted with the fully coupled GFDL SPEAR model (Delworth et al. 2020). SPEAR is built upon the GFDL AM4 atmosphere and LM4 land models (Zhao et al. 2018; Held et al. 2019), coupled with the MOM6 ocean and SIS2 sea ice models (Adcroft et al. 2019). SPEAR is specifically optimized to serve both real-time seasonal and decadal forecasts as well as uninitialized multidecadal climate projections, providing a seamless modeling framework. SPEAR has three versions that differ in horizontal resolution in the atmosphere and land components: 1° (~100 km; SPEAR_LO), 0.5° (~50 km; SPEAR_MED), and 0.25° (~25 km; SPEAR_HI). The physics are identical across these three configurations, except for modest tuning in the damping, advection, and radiative parameters in SPEAR_HI to improve the simulation of tropical cyclone intensity and maintain radiative balance. Model timesteps vary by resolution to ensure numerical stability. All versions include 33 vertical levels in the atmosphere, up to 1hPa, and are coupled to the same 1° ocean model (with tropical refinement to 1/3°). In this study, we primarily focus on SPEAR_HI, which has demonstrated notable performance in simulating extreme precipitation and relevant processes over the Northeast US (Jong et al., 2023; 2024).

To assess the effects of climate mitigation, we use simulations forced by two future radiative forcing pathways: SSP5-8.5 and SSP5-3.4OS. SSP5-8.5 represents a very high-end change in future anthropogenic GHG emissions (O'Neill et al. 2016; Riahi et al. 2017; Gidden et al. 2019; Meinshausen et al. 2020; Tebaldi et al. 2021). It served as an unmitigated baseline scenario, assuming fossil fuel-intensive economic development with minimal climate policy intervention. SSP5-8.5 has increasingly been regarded as implausible given recent climate policies and global energy transitions; in fact, observed GHG emissions have already diverged from the extreme emissions pathway in SSP5-8.5 (Hausfather and Peters 2020; Pielke et al. 2022; Hausfather and

Moore 2022; Meinshausen et al. 2022). The SSP5-8.5 scenario, nevertheless, remains valuable for understanding the physical climate responses and sensitivity to steadily increasing external forcing. It also serves as a reference for comparing with SSP5-3.4OS given the scenario design.

SSP5-3.4OS initially follows the high-emissions pathway of SSP5-8.5 until 2040, whereupon aggressive mitigation efforts are simulated to rapidly reduce GHG emissions, reaching net negative emissions by about 2070 (O'Neil et al. 2016). As a result, methane (CH_4) concentrations drop almost immediately due to its short atmospheric lifetime, while the rise in CO_2 concentrations levels off following the mitigation efforts and eventually begins to decline by the late 2050s (Fig. S1) (O'Neill et al. 2016; Riahi et al. 2017; Gidden et al. 2019; Meinshausen et al. 2020; Tebaldi et al. 2021). These reductions are hypothesized to be achieved through both a sharp drop in fossil fuel use and through the implementation of carbon capture and storage via bioenergy cropland expansion (Hurtt et al. 2020; Melnikova et al. 2022). While SSP5-3.4OS is also regarded as unrealistic due to the timing, abruptness, and scale of mitigation required, it offers a useful framework for exploring how the climate system may respond to a rapid drawdown in GHG concentrations following a temporary overshoot of global warming targets (Labe et al. 2024). The time-series of CO_2 and CH_4 concentrations, as well as GMST, under SSP5-8.5 and SSP5-3.4OS in SPEAR are shown in Fig. S1. For both SSP5-8.5 and SSP5-3.4OS, the GMST anomalies presented here are relative to the preindustrial mean taken from a control simulation with atmospheric composition fixed at levels representative of the year 1850.

Because of the high computational cost of high-resolution modeling, SPEAR_HI includes only a limited number of ensemble members (10 for SSP5-8.5 and six for SSP5-3.4OS). To better constrain internal variability (e.g., Mankin et al. 2020; Lehner and Deser 2023), we also compare results from the SPEAR_MED large ensemble, which provides 30 ensemble members. In both SPEAR_HI and SPEAR_MED, each ensemble member is initialized from different year of their respective preindustrial control simulations, spaced 20 years apart, to sample diverse phases of atmospheric and oceanic internal variability. While multiple ensemble members are used to characterize the range of internal variability, our primary focus is on the forced responses of extreme precipitation to external radiative forcing, represented by the ensemble mean. A complete list of simulations and model details used in this study is summarized in Table S1.

2.2 Definition of extreme precipitation

Extreme precipitation is defined as daily precipitation exceeding the 99th percentile of wet days (defined as ≥0.1 mm/day). The 99th percentile threshold is calculated based upon the climatology from 1951 to 2020 taken separately from SPEAR_HI or SPEAR_MED. All ensemble members and grid points within the Northeast US region are included to calculate the 99th percentile threshold for each model. As the results, the 99th percentile threshold is constant across the region and static with time for both the SSP5-8.5 and SSP5-3.4OS simulations. Extreme events are selected separately for the warm season (June to November) and the cold season (December to May). Our analysis focused on projected changes in extreme precipitation from 2021 to 2100.

2.3 The Northeast US region

The Northeast US is defined as the portion of US land within 37-50°N and 80.5-67°W. This includes the states of Maine, New Hampshire, Vermont, Massachusetts, Rhode Island, Connecticut, New York, New Jersey, Pennsylvania, Delaware, Maryland, Washington D.C., and parts of Virginia and West Virginia. Canada and ocean grid points are masked out. The Northeast US domain used here is illustrated in Figure 3.

2.4 Statistical Significance

Statistical significance of differences between two periods is tested using a bootstrapping resampling approach. We randomly reshuffle the original time series and draw two segments – each matching the length of the period analyzed – from the shuffled time series. The difference between these two randomly selected segments is then calculated. This procedure is repeated 1000 times to generate a distribution for assessing the significance of the targeted difference.

3. Results

In SSP5-8.5, the unmitigated baseline scenario, both the global warming level (Fig. S1a) and extreme precipitation frequency over the Northeast US (Fig. 1a,b) continue to linearly increase through the end of 21st century with SPEAR_HI. By definition, extreme precipitation occurs in about 1% of wet days per year in the historical period; this frequency is projected to rise to 2.3% in the warm season and 2.6% in the cold season by 2100. The rate of increase is also faster in the cold season (+0.16% per decade) than in the warm season (+0.12% per decade). In terms of absolute frequency, extreme precipitation events happened on average 2.1 days and 2.0 days per year in the warm and cold seasons, respectively, in 2001-2020. These values are projected to rise to 3.8 days and 4.2 days per year, respectively, by 2081-2100 (Table 1). While large internal variability (spread across ensemble members) exists in regional extreme precipitation, all the ensemble members of SPEAR_HI show an increasing trend in extreme precipitation frequency, indicating a robust response of extreme precipitation to rising GHG concentrations in both seasons.

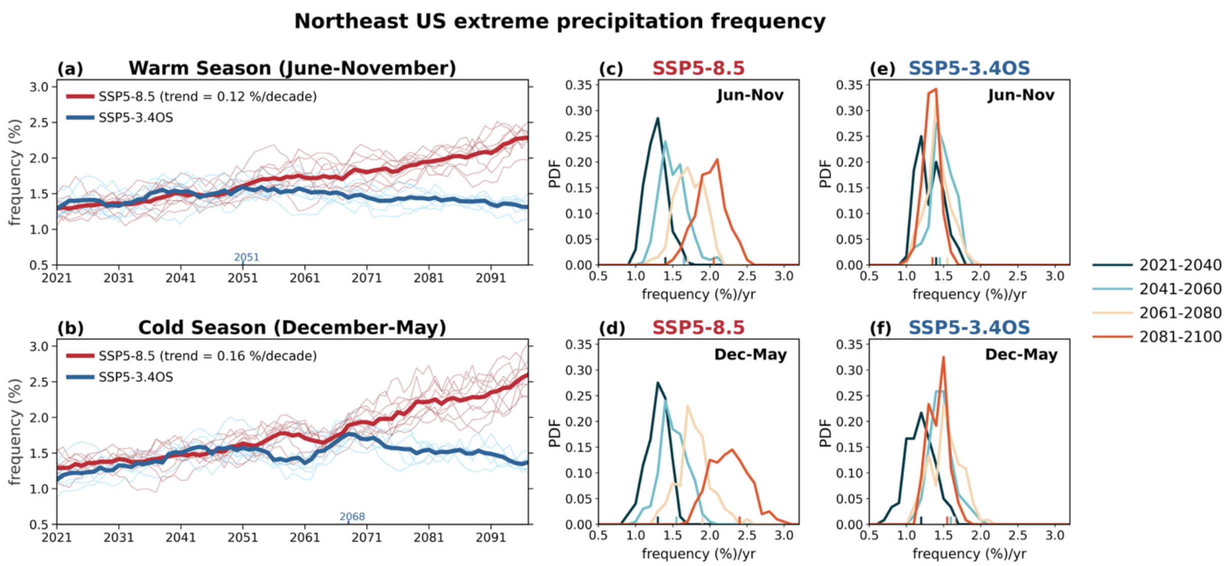

Figure 1. Changes in the frequency of extreme precipitation over the Northeast US from 2021 to 2100 in SPEAR_HI. **(a), (b)** Time-series of extreme precipitation frequency under the SSP5-8.5 (red) and SSP5-3.4OS (blue) scenarios in the **(a)** warm season (June-November) and **(b)** cold season (December-May). Thick lines represent the ensemble mean, and thin lines show individual ensemble members. All time-series are smoothed with a 7-year running mean centered on each year to remove the interannual variability. The year in which frequency peaks under SSP5-3.4OS (2051 for the warm season and 2068 for the cold season) is marked in each panel. **(c)-(f)** Changes in the distribution of extreme precipitation frequency under **(left)** SSP5-8.5 and (**right)** SSP5-3.4OS in the (**top)** warm season and **(bottom)** cold season. Each colored line presents the probability density function (PDF) of extreme precipitation frequency per year in a 20-year period. Median values of each PDF are labelled by tick marks on the x-axis.

Table 1. Average frequency and count of days of extreme precipitation events per year over the Northeast US in the **(top)** warm season and **(bottom)** cold season for different 20-year periods under the **(left)** SSP5-8.5 and **(right)** SSP5-3.4OS scenarios in SPEAR_HI. Values represent the ensemble mean of the model. For example, during 2001–2020, extreme precipitation occurred on average 1.2% of the time in the warm season, corresponding to 2.1 days per year with an extreme precipitation event somewhere in the Northeast US.

		SSP5-8.5	**SSP5-3.4OS**
Warm Season (June – November)	2001 – 2020	1.2% (2.1 days)	1.2% (2.1 days)
	2041 – 2060	1.6% (2.9 days)	1.5% (2.8 days)
	2081 – 2100	2.1% (3.8 days)	1.4% (2.5 days)
Cold Season (December – May)	2001 – 2020	1.1% (2.0 days)	1.1% (2.0 days)
	2041 – 2060	1.6% (2.9 days)	1.5% (2.8 days)
	2081 – 2100	2.3% (4.2 days)	1.5% (2.8 days)

After aggressive mitigation efforts are introduced by 2041 in SSP5-3.4OS, the GMST continues to rise and overshoots 2°C above preindustrial levels before reaching its peak in 2059 (Fig. S1a). The rate of decline in GMST following the peak is relatively slow (-0.013 °C per year) compared to the rate of warming prior to the peak (+0.038 °C per year). Consequently, even with aggressive mitigation, it takes nearly 50 years for the GMST to return to approximately 2°C of mean warming level – still warmer than the level in 2021. In response to the decline in radiative forcing, extreme precipitation frequency over the Northeast US also decreases (Fig. 1a,b), but the evolution differs between seasons. In the warm season, extreme precipitation continues to increase after 2041, peaking at about 1.6% in 2051, several years before the GMST peak, and then enters a steady decline. By 2100, the frequency is projected to fall to around 1.3%, similar to the 2021 value. All six ensemble members of SPEAR_HI experience an increasing trend prior to the peak global warming level and then a decreasing trend afterward, suggesting a robust physical signal. In contrast to the warm season evolution, the cold-season response is more delayed. Extreme precipitation stops increasing shortly after the mitigation is implemented, before rising again slightly to around 1.8% by 2068. After that, it declines steadily to approximately 1.4% by 2100. Five of the six ensemble members exhibit a similar evolution, suggesting a robust response across the ensemble members. In terms of absolute frequency, under SSP5-3.4OS, warm-season extreme precipitation events are projected to occur on average 2.5 days per year by 2081-2100 – not yet returning to the mean 2001-2020 level, but lower than mid-21st century. For the cold season, extreme precipitation events are projected to occur on average 2.8 days per year by 2081-2100, recovering only to mid-21st century level (Table 1).

To address the limited ensemble size in SPEAR_HI, we also examined the parallel 30-member ensemble from SPEAR_MED (Fig. S2a,b). SPEAR_MED presents highly consistent results: in the warm season, extreme precipitation continues to increase after 2041 and reverses its trend in 2052, a few years before the peak warming. The frequency peaks at around 1.6% before declining steadily to around 1.3% by 2100. In the cold season, the increasing trend in extreme precipitation slows shortly after the mitigation begins, followed by a modest rise to a peak of about 1.7% around 2070. Afterward, extreme precipitation declines to approximately 1.4% by the end of the century.

The benefit of mitigation and seasonal differences in response are more evident when examining the probability distributions of extreme precipitation frequency. Figures 1c-f show the probability density functions (PDFs) of extreme precipitation frequency (per year) for each season over 20-year periods. In SSP5-8.5, the PDFs shift steadily to the right, indicating higher frequencies over time. In the warm season (Fig. 1c), the median frequency is 1.4% per year in 2021-2040 and increases to 2.1% per year in 2081-2100. The shift is even more pronounced in the cold season (Fig. 1d), where the median frequency rises from 1.3% per year in 2021-2040 to 2.4% per year in 2081-2100. In contrast, in SSP5-3.4OS, the rightward shift in the warm-season PDF – that is, the increase in extreme precipitation frequency – slows shortly after the mitigation begins in 2041 (Fig. 1e), compared to the shift in SSP5-8.5. By 2081-2100, the PDF nearly returns to the 2021-2040 distribution, with medians around 1.4% per year in both periods. In the cold season, the slowdown in the rightward shift of the PDF is delayed, compared to in the warm season (Fig. 1f). The PDF for 2041-2060 still presents a clear rightward shift relative to 2021-2040, and the shift continues until 2061-2081. By 2081-2100, the cold-season PDF returns to a state resembling the mid-21st century, with medians around 1.6% per year.

These results are even more apparent in the 30-member SPEAR_MED ensemble (Fig. S2c-f). Under SSP5-8.5, the cold-season PDFs exhibit a more pronounced rightward shift – that is, larger increases in extreme precipitation frequency – over time than the warm-season PDFs (Fig. S2c-d). Under SSP5-3.4OS, the reduction in GHG concentrations limits the rightward shift in PDFs by curbing continued warming, but the seasonal distinction remains. By 2081-2100, the warm-season PDF resembles that of 2021-2040, whereas the cold-season PDF only recovers to the 2041-2060 distribution (Fig. S2e-f), reflecting a delayed response of cold-season extreme precipitation to reduced GHG forcing.

To further understand the relationship between Northeast US extreme precipitation and global mean warming, we next scale extreme precipitation frequency by its corresponding GMST anomaly (Fig. 2 and Fig. S3). Consistent with recent studies (e.g., Boucher et al. 2012; Melnikova et al. 2023; Pfleiderer et al. 2024; Roldán-Gómez et al. 2025), this approach allows us to assess whether the response of extremes follows the magnitude of global warming or exhibits hysteresis behavior. In the warm season, the frequency increases by 0.25% per degree of global warming under SSP5-8.5 (Fig. 2a). Under SSP5-3.4OS, shortly before the GMST reaches its peak warming of 2.6 °C in 2059, the frequency starts to decline with time in SPEAR_HI (Fig. 2b). Notably, at the same warming level, the frequency after the peak warming is even lower than before the peak warming, suggesting an "overcompensated" behavior (e.g., Pfleiderer et al. 2024). Because the GMST cooling rate is slower than the warming rate (Fig. S1a), the 30-year average extreme precipitation in the warm season is nearly identical when comparing before and after the peak warming (difference of 0.01%, not statistically significant at the 95% confidence level). Unsurprisingly, the relationship between extreme precipitation frequency and GMST is not entirely linear, with some fluctuations – particularly under SSP5-3.4OS – primarily due to the limited number of ensemble members in SPEAR_HI and subsequent lower signal-to-noise. Given this concern, the 30-member SPEAR_MED ensemble (Fig. S3a,b) provides a clearer view, confirming that the mitigation efforts effectively slow and eventually reverse the trend of extreme precipitation frequency in the Northeast US during the warm season.

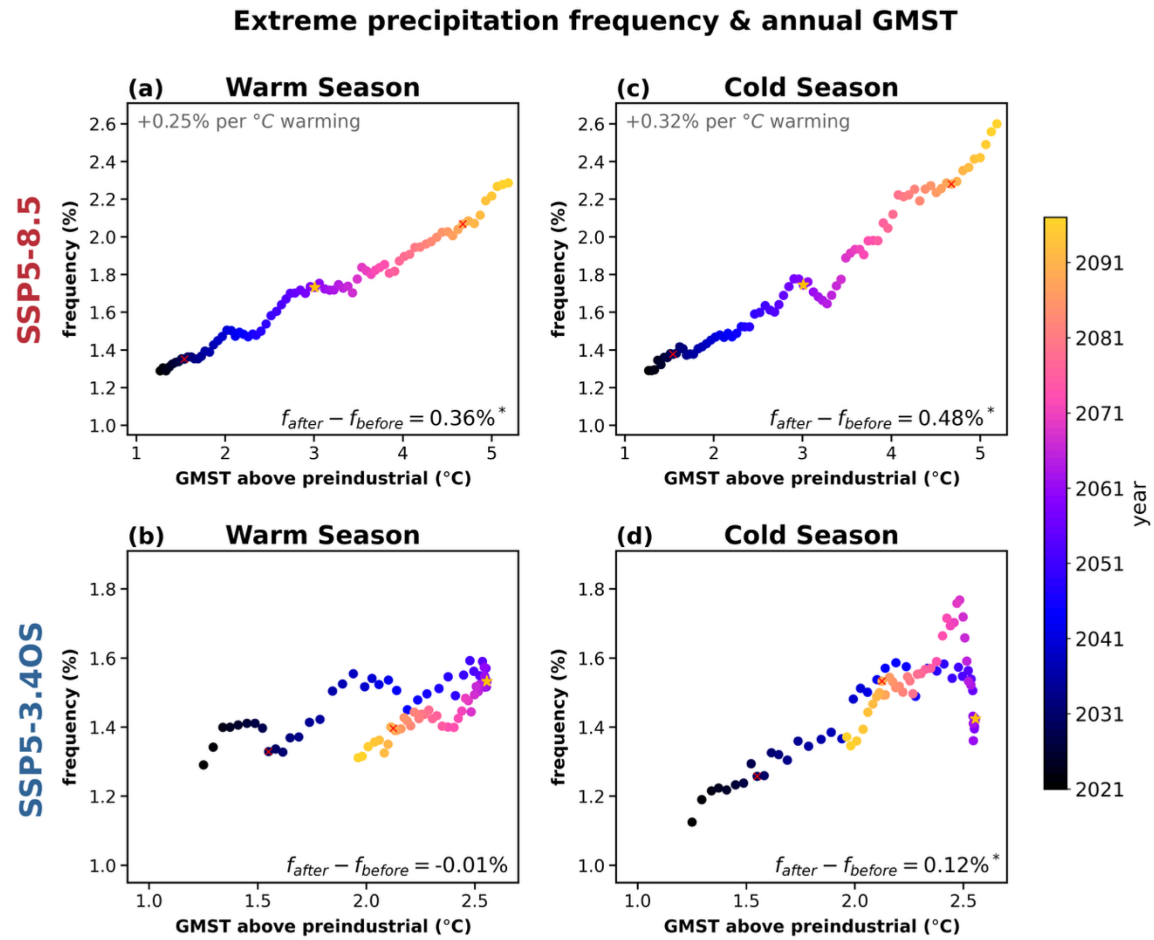

Figure 2. Changes in extreme precipitation frequency as a function of GMST anomaly in **(top)** SSP5-8.5 and **(bottom)** SSP5-3.4OS, for the **(left)** warm season and **(right)** cold season. Each dot represents the ensemble mean from SPEAR_HI for a given year, with color indicating the year. Both GMST and frequency are smoothed with a 7-year running mean centered on each year. The difference in the 30-year average frequency before and after the peak warming year under SSP5-3.4OS is shown in the lower-right corner of each panel. Asterisks denote statistically significant differences between the two periods at the 95% confidence level. The point corresponding to the peak warming year (2059) under SSP5-3.4OS is marked with a yellow star, and red crosses indicate the years 30 years before and after the peak.

As described earlier, a different story emerges in the cold season, however. For a baseline warming comparison, we found that the frequency of extreme precipitation increases by 0.32% per degree of warming in SSP5-8.5 in SPEAR_HI. This is faster than the rate of change in the warm season (Fig. 2c). On the other hand, in SSP5-3.4OS, extreme precipitation frequency briefly drops but rebounds within a few years immediately after the peak warming of 2.6°C in 2059 as the GMST starts to cool (Fig. 2d). It is not until around 2068, when the warming level drops to 2.4°C, that the frequency of extreme precipitation begins a steady decline with decreasing GMST and total radiative forcing. As a result, the 30-year average frequency after the peak warming remains statistically significantly higher than the 30-year average frequency before the peak warming by about 0.12%. This behavior is consistent with Roldan-Gomez et al. (2025), which noted that the relationship between regional extreme precipitation and GMST is similar before and after the peak global warming, except for a transition period immediately after the peak warming where the two variables become decoupled (~2059-2068 in our case). After this transition period, the relationship realigns, but the elevated frequencies accumulated during the transition period remain. Consequently, extreme precipitation frequency is significantly higher after the peak warming than before, even at equivalent GMST levels.

The consistency found in the 30-member SPEAR_MED ensemble (Fig. S3b,d) reinforces the likelihood of this behavior as simulated in the SPEAR models. Unlike the warm season, where extreme precipitation frequency declines monotonically with GMST shortly before the peak warming and continues thereafter, the cold season experiences a transition period in which its frequency and the GMST are decoupled before eventually resuming a concurrent declining trend. Because of this lagged response, at the same warming level, the post-peak extreme precipitation frequency remains higher than the pre-peak frequency, at least until 2100 – the end of the SPEAR simulations. This contrasts with the extreme precipitation-GMST relationship in the warm season, where the post-peak frequency is lower than the pre-peak frequency at the same warming level.

Changes in extreme precipitation vary not only seasonally but also spatially. Figure 3 presents the changes in extreme precipitation frequency across the Northeast US region. Under SSP5-8.5 (Fig. 3a,c), the faster increase in extreme precipitation in the cold season occurs broadly across the region. At the same time, distinct regional patterns emerge within each season: in the warm season, increases are more pronounced in inland regions compared to coastal regions; while in the cold season, changes are more spatially uniform but largest in the Mid-Atlantic region (e.g., Maryland

and Virginia). Consistent with earlier results, the spatial distribution of changes in extreme precipitation exhibits strong seasonal distinctions in SSP5-3.4OS (Fig. 3b,d). In the warm season, the 30-year average extreme precipitation frequency after the peak warming is not statistically significantly different from that before the peak warming throughout the Northeast. In the cold season, in line with earlier findings (e.g., Fig. 2d), extreme precipitation frequency remains higher after the peak warming than before. This behavior, however, is not uniform across the region. For instance, the lagged declines are primarily confined to the southern part of the Northeast (the Mid-Atlantic region and southeastern Pennsylvania) and areas along Lake Ontario. In these areas, the 30-year average frequency after the peak warming is approximately 0.4% per year higher than the 30-year average frequency before the peak warming, and the differences are statistically significantly at the 95% confidence level. These results highlight that the response of extreme precipitation to sudden declines in GHGs may be modulated by both seasonal large-scale mean state conditions and with spatial heterogeneity across the Northeast region.

This marked spatial heterogeneity suggests that major urban areas within the Northeast may experience distinct changes in extreme precipitation in a plausible future with aggressive global climate mitigation efforts. The delayed response seen in SSP5-3.4OS during the cold season is particularly concentrated in the southern coastal region (Fig. 3d), motivating a closer examination of three representative cities along the highly populated Northeast corridor – Boston, New York City, and Baltimore. We also include Rochester given its proximity downstream of Lake Ontario, where similar delays in extreme precipitation frequency change are evident. For these four cities, we examine how cold-season extreme precipitation frequency evolves over time (Fig. S4) and its statistical relationship relative of the GMST (Fig. 4) under SSP5-3.4OS.

In Boston, located in the northern coastal Northeast, extreme precipitation frequency starts to decline soon after the mitigation is implemented, despite some temporal fluctuations that are typical at this regional scale (Fig. S4c). By the end of the 21st century, the frequency of extreme precipitation returns to those comparable with around 2021. The 30-year average frequency after the peak warming is also not statistically significantly different from that of before (Fig. 4c). These findings suggest that the aggressive mitigation in SSP5-3.4OS could effectively reverse the upward trend in extremes and restore them to near-present day levels in some regions such as Boston.

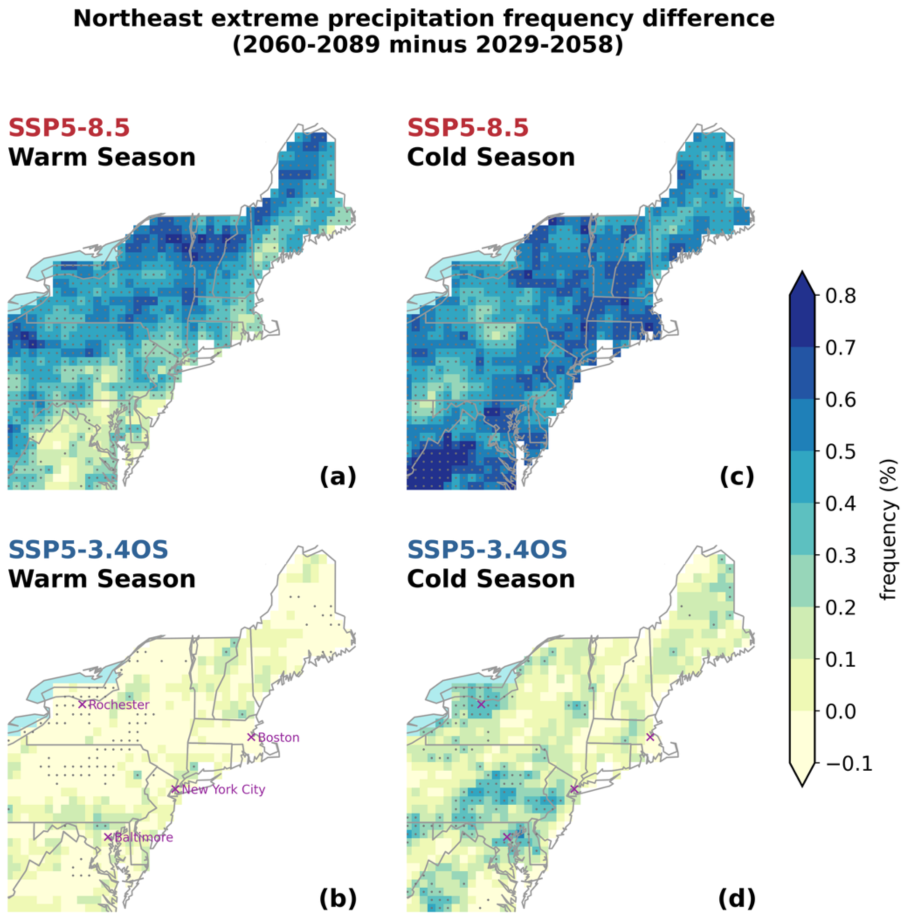

Figure 3. Spatial changes in extreme precipitation frequency across the Northeast US in SPEAR_HI, showing the difference in 30-year average frequency before and after the peak warming year under SSP5-3.4OS (2059) under **(top)** SSP5-8.5 and **(bottom)** SSP5-3.4OS, for the **(left)** warm season and **(right)** cold season. The values presented are averaged percentages per year. Dots denote statistically significant differences between the two periods at the 95% confidence level. The locations of the cities analyzed in Figures S4 and 4 are indicated in the bottom panels.

The reversal in the increasing extreme precipitation frequency, however, becomes more delayed as one moves southward (Fig. 3d). For example, in New York City, located in the central coastal Northeast, extreme precipitation frequency starts to decline later than in Boston (Fig. S4c,d). The cold-season frequency starts to decline a few years after the peak warming (Fig. 4d); owing to this delay, the post-peak 30-year average frequency remains significantly higher than that of before.

Further southward, Baltimore exhibits a substantially delayed response in extreme precipitation frequency. Its cold-season extreme precipitation continues to rise even after the mitigation starts and global mean warming is well past peaks (Fig. S4b and Fig. 4b), with frequencies not beginning a steady decline until around 2070. Consequently, the 30-year average frequency after the peak warming remains about 0.33% per year higher than before – a considerable difference given that extreme precipitation is defined by the top 1% of historical daily precipitation events. This implies that Baltimore experiences nearly 30% more frequent extremes even in a world with strong climate mitigation efforts.

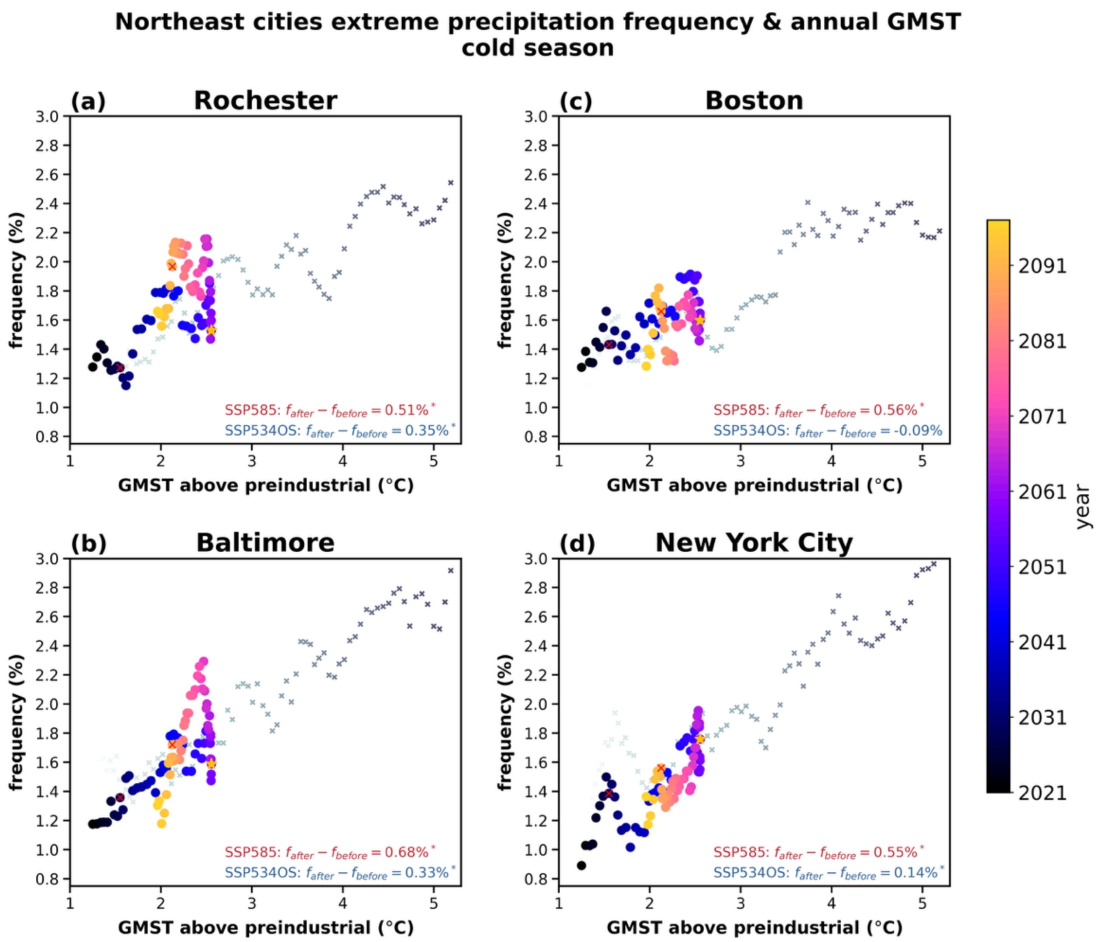

Figure 4. Changes in extreme precipitation frequency as a function of GMST anomaly during the cold season in **(a)** Rochester, **(b)** Baltimore, **(c)** Boston, and **(d)** New York City. Colored dots represent SSP5-3.4OS and grey crosses represent SSP5-8.5. Each symbol shows the ensemble

mean from SPEAR_HI for a given year, with color indicating the year. Both GMST and frequency are smoothed with a 7-year running mean centered on each year. The difference in the 30-year average frequency before and after the peak warming year under SSP5-3.4OS is shown in the lower-right corner of each panel. Asterisks indicate statistically significant differences between the two periods at the 95% confidence level. The point corresponding to the peak warming year (2059) under SSP5-3.4OS is marked with a yellow star, and red crosses indicate the years 30 years before and after the peak.

A comparable lag is seen in Rochester, where no clear decline in extreme precipitation frequency emerges until roughly 2085 (Fig. S4a and Fig. 4a). One plausible explanation is the influence of orography and proximity to the lake shore. Rochester lies downstream of Lake Ontario, whose surface cools more slowly than land and the GMST. This thermal inertia means that, even as global temperatures begin to fall, the warmer lake could enhance the available moisture content for synoptic-scale winter storms and lake-effect precipitation, potentially sustaining higher extreme precipitation frequencies in the region into the future. While more work is needed to delve into why the responses to mitigation differ across these regions, lake enhancement could be an important factor in Rochester's distinct behavior.

4. Conclusion and discussion

As climate mitigation strategies are increasingly proposed in order to reduce atmospheric GHG concentrations, it is becoming even more crucial to understand how various aspects of the climate system may respond to such rapid carbon reductions. In this study, we examine potential changes in extreme precipitation over the Northeast US in an overshoot scenario called SSP5-3.4OS, which is simulated by the fully coupled 25-km GFDL SPEAR_HI model.

Our results suggest that the increasing trend in extreme precipitation frequency over the Northeast US, driven by anthropogenic GHG forcing, slows and eventually reverses following reductions in GHG levels. The timing of this reversal, however, is seasonally and regionally dependent. In the warm season, extreme precipitation frequency begins to decline shortly after the implementation of mitigation efforts starting in 2041, returning to levels comparable to those of the early 21st century by the end of 21st century. On the other hand, the cold-season response is delayed, and a steady decline in extreme precipitation frequency does not emerge until approximately a decade after the peak global warming. This delay reflects a hysteresis effect, whereby, at equivalent warming levels, cold-season extreme precipitation remains more frequent after the peak warming than before. By the end of the 21st century, cold-season extreme precipitation frequency recovers only to levels equivalent to earlier in the mid-21st century. This delayed response in the cold season also exhibits pronounced spatial differences. Urban areas in the southern Northeast, such as Baltimore, and far inland locations like Rochester may be more likely to experience this delayed response than northern cities such as New York City and Boston.

One plausible explanation for the differing responses between the warm and cold seasons is that cold-season extreme precipitation over the Northeast US is largely associated with extratropical cyclones (Agel et al. 2018; Huang et al. 2018), where dynamical processes play a central role. As a result, changes in cold-season extreme precipitation are less directly constrained by the global warming level. In addition, Delworth et al. (2022) showed that under SSP5-3.4OS, the AMOC continues to weaken well after GMST peaks, and this persistent weakening AMOC can modulate large-scale atmospheric circulations in the cold season, influencing the tracks of extratropical storms. Such processes may contribute to the seasonally distinct behavior in extreme precipitation changes. While further research is needed to confirm the mechanisms that drive these seasonal differences, our findings reflect that regional responses of extremes to GHG reductions can be modulated by seasonality, local-scale processes, and other factors, leading to nonlinear behaviors. This underscores the need for targeted and region-specific assessments.

A caveat of this study is that it relies on a single climate model. Previous work has shown that many aspects of climate system's response under SSP5-3.4OS exhibit varying degrees of inter-model spread among several CMIP6 models (Pfleiderer et al., 2024), including large differences in the level of hysteresis in GMST. Our model choice was limited by the availability of fully coupled climate models with higher horizontal resolution that better resolve physical processes relevant to extreme precipitation (e.g., Murakami et al. 2015; Iles et al. 2020; Stansfield et al. 2020; Jong et al. 2023; Lee et al. 2025), as well as the need for multiple ensemble members to characterize a wide range of possible future realizations (e.g., Deser 2020; Mankin et al. 2020; Jong et al. 2023). Nevertheless, our results are qualitatively similar to those of Pfleiderer et al.

(2024), who found that most of the models simulate a post-mitigation decrease in extreme precipitation frequency over the eastern US, although some show overcompensation behavior. Future work focusing on the physical processes underlying the differing responses between warm- and cold-season extremes over the Northeast US will help strengthen the results drawn from the SPEAR_HI simulations.

Another limitation is that the SSP5-3.4OS simulation in SPEAR_HI only extends through 2100. While both warm and cold-season extreme precipitation over the Northeast US start to decline steadily before 2100, neither has returned to the 1951-2020 climatological baseline. It is therefore unclear whether extreme precipitation will eventually fully recover to preindustrial levels under net-zero GHG emissions, and on what timescale. This uncertainty stems largely from slow ocean processes and lagged ocean temperature warming caused by changes in the overturning circulation (e.g., Held et al. 2010; Armour et al. 2016; Ceppi et al. 2018; King et al. 2024). For example, using an Earth System Model with 1000-year experiments, King et al., (2024) showed that although the GMST initially cools in response to a rapid shift to net-zero emissions, after about 50 years, it reverses the trend and gradually warms due to oceanic influences. Lagged oceanic responses also appear in projections of AMOC recovery. In the GFDL SPEAR model under SSP5-3.4OS, the AMOC weakening, initially driven by external forcing, only begins to stabilize by the end of 21st century (Delworth et al. 2022). Given that the AMOC influences global SST patterns and therefore large-scale atmospheric circulations considerably, it remains unclear how AMOC's response to climate mitigation will influence regional climate extremes beyond 2100. Thus, simulations ending in 2100 cannot fully capture whether the projected responses to mitigation in the late 21st century might reverse or change beyond 2100 due to slow ocean processes.

These limitations, together with our results, highlight the complexity of how global climate mitigation might influence the future climate system. Further research that examines responses to various overshooting pathways and mitigation strategies – across multiple timescales and spatial scales – along with process-oriented studies, will be crucial for advancing our understanding of how the climate system responds to GHG reductions. Such efforts can help policymakers, scientists, and other stakeholders implement mitigation measures more effectively and develop resilient and actionable plans for communities. In particular, urban areas with dense populations and infrastructure can benefit from adaptation strategies that specifically address localized flood risks and runoff concerns that are associated with extreme precipitation.

Acknowledgments

We thank Dr. Kristina Dahl (Climate Central, Inc) for reviewing our study. Bor-Ting Jong received award NA23OAR4320198 from the National Oceanic and Atmospheric Administration, U.S. Department of Commerce. We acknowledge GFDL resources made available for this research. The statements, findings, conclusions, and recommendations are those of the author(s) and do not necessarily reflect the views of the National Oceanic and Atmospheric Administration, or the U.S. Department of Commerce.

Data availability

SPEAR_HI and SPEAR_MED are described in Delworth et al., 2020, Jong et al., 2023, and at https://www.gfdl.noaa.gov/spear/. All data for this study is available at https://zenodo.org/records/17237074 (Jong et al. 2025). Daily precipitation data from SPEAR_MED Large Ensembles are available at https://www.gfdl.noaa.gov/spear_large_ensembles/.

Conflict of interest

The authors declare no conflict of interest relevant to this study.

Reference

Adcroft, A., and Coauthors, 2019: The GFDL Global Ocean and Sea Ice Model OM4.0: Model Description and Simulation Features. *Journal of Advances in Modeling Earth Systems*, **11**, 3167–3211, https://doi.org/10.1029/2019MS001726.

Agel, L., M. Barlow, J.-H. Qian, F. Colby, E. Douglas, and T. Eichler, 2015: Climatology of Daily Precipitation and Extreme Precipitation Events in the Northeast United States. *Journal of Hydrometeorology*, **16**, 2537–2557, https://doi.org/10.1175/JHM-D-14-0147.1.

——, ——, S. B. Feldstein, and W. J. Gutowski, 2018: Identification of large-scale meteorological patterns associated with extreme precipitation in the US northeast. *Clim Dyn*, **50**, 1819–1839, https://doi.org/10.1007/s00382-017-3724-8.

An, S.-I., J. Shin, S.-W. Yeh, S.-W. Son, J.-S. Kug, S.-K. Min, and H.-J. Kim, 2021: Global Cooling Hiatus Driven by an AMOC Overshoot in a Carbon Dioxide Removal Scenario. *Earth's Future*, **9**, e2021EF002165, https://doi.org/10.1029/2021EF002165.

Armour, K. C., J. Marshall, J. R. Scott, A. Donohoe, and E. R. Newsom, 2016: Southern Ocean warming delayed by circumpolar upwelling and equatorward transport. *Nature Geosci*, **9**, 549–554, https://doi.org/10.1038/ngeo2731.

Asadieh, B., and N. Y. Krakauer, 2015: Global trends in extreme precipitation: climate models versus observations. *Hydrology and Earth System Sciences*, **19**, 877–891, https://doi.org/10.5194/hess-19-877-2015.

Azar, C., D. J. A. Johansson, and N. Mattsson, 2013: Meeting global temperature targets—the role of bioenergy with carbon capture and storage. *Environ. Res. Lett.*, **8**, 034004, https://doi.org/10.1088/1748-9326/8/3/034004.

Boucher, O., and Coauthors, 2012: Reversibility in an Earth System model in response to CO2 concentration changes. *Environ. Res. Lett.*, **7**, 024013, https://doi.org/10.1088/1748-9326/7/2/024013.

Brown, P. J., R. S. Bradley, and F. T. Keimig, 2010: Changes in Extreme Climate Indices for the Northeastern United States, 1870–2005. *Journal of Climate*, **23**, 6555–6572, https://doi.org/10.1175/2010JCLI3363.1.

Cao, L., G. Bala, and K. Caldeira, 2011: Why is there a short-term increase in global precipitation in response to diminished CO2 forcing? *Geophysical Research Letters*, **38**, https://doi.org/10.1029/2011GL046713.

Ceppi, P., G. Zappa, T. G. Shepherd, and J. M. Gregory, 2018: Fast and Slow Components of the Extratropical Atmospheric Circulation Response to CO2 Forcing. *Journal of Climate*, **31**, 1091–1105, https://doi.org/10.1175/JCLI-D-17-0323.1.

Chadwick, R., P. Wu, P. Good, and T. Andrews, 2013: Asymmetries in tropical rainfall and circulation patterns in idealised CO2 removal experiments. *Clim Dyn*, **40**, 295–316, https://doi.org/10.1007/s00382-012-1287-2.

Crossett, C. C., L.-A. L. Dupigny-Giroux, K. E. Kunkel, A. K. Betts, and A. Bomblies, 2023: Synoptic Typing of Multiduration, Heavy Precipitation Records in the Northeastern United States: 1895–2017. *Journal of Applied Meteorology and Climatology*, **62**, 721–736, https://doi.org/10.1175/JAMC-D-22-0091.1.

DeGaetano, A. T., 2009: Time-Dependent Changes in Extreme-Precipitation Return-Period Amounts in the Continental United States. *Journal of Applied Meteorology and Climatology*, **48**, 2086–2099, https://doi.org/10.1175/2009JAMC2179.1.

——, and C. M. Castellano, 2017: Future projections of extreme precipitation intensity-duration-frequency curves for climate adaptation planning in New York State. *Climate Services*, **5**, 23–35, https://doi.org/10.1016/j.cliser.2017.03.003.

——, G. Mooers, and T. Favata, 2020: Temporal Changes in the Areal Coverage of Daily Extreme Precipitation in the Northeastern United States Using High-Resolution Gridded Data. *Journal of Applied Meteorology and Climatology*, **59**, 551–565, https://doi.org/10.1175/JAMC-D-19-0210.1.

Delworth, T. L., and Coauthors, 2020: SPEAR: The Next Generation GFDL Modeling System for Seasonal to Multidecadal Prediction and Projection. *Journal of Advances in Modeling Earth Systems*, **12**, e2019MS001895, https://doi.org/10.1029/2019MS001895.

——, W. F. Cooke, V. Naik, D. Paynter, and L. Zhang, 2022: A weakened AMOC may prolong greenhouse gas–induced Mediterranean drying even with significant and rapid climate change mitigation. *Proceedings of the National Academy of Sciences*, **119**, e2116655119, https://doi.org/10.1073/pnas.2116655119.

Deser, C., 2020: "Certain Uncertainty: The Role of Internal Climate Variability in Projections of Regional Climate Change and Risk Management". *Earth's Future*, **8**, e2020EF001854, https://doi.org/10.1029/2020EF001854.

Diffenbaugh, N. S., E. A. Barnes, and P. W. Keys, 2023: Probability of continued local-scale warming and extreme events during and after decarbonization. *Environ. Res.: Climate*, **2**, 021003, https://doi.org/10.1088/2752-5295/accf2f.

Donat, M. G., and Coauthors, 2013: Updated analyses of temperature and precipitation extreme indices since the beginning of the twentieth century: The HadEX2 dataset. *Journal of Geophysical Research: Atmospheres*, **118**, 2098–2118, https://doi.org/10.1002/jgrd.50150.

Donat, M. G., A. L. Lowry, L. V. Alexander, P. A. O'Gorman, and N. Maher, 2016: More extreme precipitation in the world's dry and wet regions. *Nature Clim Change*, **6**, 508–513, https://doi.org/10.1038/nclimate2941.

Dunn, R. J. H., and Coauthors, 2020: Development of an Updated Global Land In Situ-Based Data Set of Temperature and Precipitation Extremes: HadEX3. *Journal of Geophysical Research: Atmospheres*, **125**, e2019JD032263, https://doi.org/10.1029/2019JD032263.

Ehlert, D., and K. Zickfeld, 2018: Irreversible ocean thermal expansion under carbon dioxide removal. *Earth System Dynamics*, **9**, 197–210, https://doi.org/10.5194/esd-9-197-2018.

Fischer, E. M., and R. Knutti, 2015: Anthropogenic contribution to global occurrence of heavy-precipitation and high-temperature extremes. *Nature Clim Change*, **5**, 560–564, https://doi.org/10.1038/nclimate2617.

——, and ——, 2016: Observed heavy precipitation increase confirms theory and early models. *Nature Clim Change*, **6**, 986–991, https://doi.org/10.1038/nclimate3110.

Forster, P. M., and Coauthors, 2025: Indicators of Global Climate Change 2024: annual update of key indicators of the state of the climate system and human influence. *Earth System Science Data*, **17**, 2641–2680, https://doi.org/10.5194/essd-17-2641-2025.

Fowler, A. M., and K. J. Hennessy, 1995: Potential impacts of global warming on the frequency and magnitude of heavy precipitation. *Nat Hazards*, **11**, 283–303, https://doi.org/10.1007/BF00613411.

Frei, A., K. E. Kunkel, and A. Matonse, 2015: The Seasonal Nature of Extreme Hydrological Events in the Northeastern United States. *Journal of Hydrometeorology*, **16**, 2065–2085, https://doi.org/10.1175/JHM-D-14-0237.1.

Gasser, T., C. Guivarch, K. Tachiiri, C. D. Jones, and P. Ciais, 2015: Negative emissions physically needed to keep global warming below 2 °C. *Nat Commun*, **6**, 7958, https://doi.org/10.1038/ncomms8958.

Gidden, M. J., and Coauthors, 2019: Global emissions pathways under different socioeconomic scenarios for use in CMIP6: a dataset of harmonized emissions trajectories through the end of the century. *Geoscientific Model Development*, **12**, 1443–1475, https://doi.org/10.5194/gmd-12-1443-2019.

Guilbert, J., A. K. Betts, D. M. Rizzo, B. Beckage, and A. Bomblies, 2015: Characterization of increased persistence and intensity of precipitation in the northeastern United States. *Geophysical Research Letters*, **42**, 1888–1893, https://doi.org/10.1002/2015GL063124.

Hausfather, Z., 2025: An assessment of current policy scenarios over the 21st century and the reduced plausibility of high-emissions pathways. *Dialogues on Climate Change*, **2**, 26–32, https://doi.org/10.1177/29768659241304854.

——, and G. P. Peters, 2020: Emissions – the 'business as usual' story is misleading. *Nature*, **577**, 618–620, https://doi.org/10.1038/d41586-020-00177-3.

——, and F. C. Moore, 2022: Net-zero commitments could limit warming to below 2 °C. *Nature*, **604**, 247–248, https://doi.org/10.1038/d41586-022-00874-1.

Hayhoe, K., and Coauthors, 2007: Past and future changes in climate and hydrological indicators in the US Northeast. *Clim Dyn*, **28**, 381–407, https://doi.org/10.1007/s00382-006-0187-8.

Held, I. M., M. Winton, K. Takahashi, T. Delworth, F. Zeng, and G. K. Vallis, 2010: Probing the Fast and Slow Components of Global Warming by Returning Abruptly to Preindustrial Forcing. *Journal of Climate*, **23**, 2418–2427, https://doi.org/10.1175/2009JCLI3466.1.

Held, I. M., and Coauthors, 2019: Structure and Performance of GFDL's CM4.0 Climate Model. *Journal of Advances in Modeling Earth Systems*, **11**, 3691–3727, https://doi.org/10.1029/2019MS001829.

Henny, L., C. D. Thorncroft, and L. F. Bosart, 2022: Changes in Large-Scale Fall Extreme Precipitation in the Mid-Atlantic and Northeast United States, 1979–2019. *Journal of Climate*, **35**, 6647–6670, https://doi.org/10.1175/JCLI-D-21-0953.1.

——, ——, and ——, 2023: Changes in Seasonal Large-Scale Extreme Precipitation in the Mid-Atlantic and Northeast United States, 1979–2019. *Journal of Climate*, **36**, 1017–1042, https://doi.org/10.1175/JCLI-D-22-0088.1.

Hoerling, M., J. Eischeid, J. Perlwitz, X.-W. Quan, K. Wolter, and L. Cheng, 2016: Characterizing Recent Trends in U.S. Heavy Precipitation. *Journal of Climate*, **29**, 2313–2332, https://doi.org/10.1175/JCLI-D-15-0441.1.

Howarth, M. E., C. D. Thorncroft, and L. F. Bosart, 2019: Changes in Extreme Precipitation in the Northeast United States: 1979–2014. *Journal of Hydrometeorology*, **20**, 673–689, https://doi.org/10.1175/JHM-D-18-0155.1.

Huang, H., J. M. Winter, E. C. Osterberg, R. M. Horton, and B. Beckage, 2017: Total and Extreme Precipitation Changes over the Northeastern United States. *Journal of Hydrometeorology*, **18**, 1783–1798, https://doi.org/10.1175/JHM-D-16-0195.1.

——, ——, and ——, 2018: Mechanisms of Abrupt Extreme Precipitation Change Over the Northeastern United States. *Journal of Geophysical Research: Atmospheres*, **123**, 7179–7192, https://doi.org/10.1029/2017JD028136.

Huntingford, C., and J. Lowe, 2007: 'Overshoot' Scenarios and Climate Change. *Science*, **316**, 829–829, https://doi.org/10.1126/science.316.5826.829b.

Hurtt, G. C., and Coauthors, 2020: Harmonization of global land use change and management for the period 850–2100 (LUH2) for CMIP6. *Geoscientific Model Development*, **13**, 5425–5464, https://doi.org/10.5194/gmd-13-5425-2020.

Hwang, J., and Coauthors, 2024: Asymmetric hysteresis response of mid-latitude storm tracks to CO2 removal. *Nat. Clim. Chang.*, **14**, 496–503, https://doi.org/10.1038/s41558-024-01971-x.

Iles, C. E., R. Vautard, J. Strachan, S. Joussaume, B. R. Eggen, and C. D. Hewitt, 2020: The benefits of increasing resolution in global and regional climate simulations for European climate extremes. *Geoscientific Model Development*, **13**, 5583–5607, https://doi.org/10.5194/gmd-13-5583-2020.

IPCC, 2022: *Summary for policymakers. In Climate Change 2022: Mitigation of Climate Change. Contribution of Working Group III to the Sixth Assessment Report of the Intergovernmental Panel on Climate Change*. Cambridge University Press 1–48pp.

Jeltsch-Thömmes, A., T. F. Stocker, and F. Joos, 2020: Hysteresis of the Earth system under positive and negative CO2 emissions. *Environ. Res. Lett.*, **15**, 124026, https://doi.org/10.1088/1748-9326/abc4af.

Jong, B.-T., H. Murakami, T. L. Delworth, and W. F. Cooke, 2024: Contributions of Tropical Cyclones and Atmospheric Rivers to Extreme Precipitation Trends Over the Northeast US. *Earth's Future*, **12**, e2023EF004370, https://doi.org/10.1029/2023EF004370.

Jong, B.-T., T. L. Delworth, W. F. Cooke, K.-C. Tseng, and H. Murakami, 2023: Increases in extreme precipitation over the Northeast United States using high-resolution climate model simulations. *npj Clim Atmos Sci*, **6**, 1–9, https://doi.org/10.1038/s41612-023-00347-w.

Jong, B.-T., Z. M. Labe, T. L. Delworth, and W. F. Cooke, 2025: Northeast US Extreme Precipitation Projected Changes in SSP5-3.4OS in GFDL SPEAR. [*Dataset*] Zenodo, https://doi.org/10.5281/zenodo.17237074.

Kikstra, J. S., and Coauthors, 2022: The IPCC Sixth Assessment Report WGIII climate assessment of mitigation pathways: from emissions to global temperatures. *Geoscientific Model Development*, **15**, 9075–9109, https://doi.org/10.5194/gmd-15-9075-2022.

Kim, S.-K., J. Shin, S.-I. An, H.-J. Kim, N. Im, S.-P. Xie, J.-S. Kug, and S.-W. Yeh, 2022: Widespread irreversible changes in surface temperature and precipitation in response to CO2 forcing. *Nat. Clim. Chang.*, **12**, 834–840, https://doi.org/10.1038/s41558-022-01452-z.

King, A. D., and Coauthors, 2024: Exploring climate stabilisation at different global warming levels in ACCESS-ESM-1.5. *Earth System Dynamics*, **15**, 1353–1383, https://doi.org/10.5194/esd-15-1353-2024.

Kopparla, P., E. M. Fischer, C. Hannay, and R. Knutti, 2013: Improved simulation of extreme precipitation in a high-resolution atmosphere model. *Geophysical Research Letters*, **40**, 5803–5808, https://doi.org/10.1002/2013GL057866.

Kotz, M., S. Lange, L. Wenz, and A. Levermann, 2024: Constraining the Pattern and Magnitude of Projected Extreme Precipitation Change in a Multimodel Ensemble. *Journal of Climate*, **37**, 97–111, https://doi.org/10.1175/JCLI-D-23-0492.1.

Koven, C. D., and Coauthors, 2022: Multi-century dynamics of the climate and carbon cycle under both high and net negative emissions scenarios. *Earth System Dynamics*, **13**, 885–909, https://doi.org/10.5194/esd-13-885-2022.

Kunkel, K. E., D. R. Easterling, D. A. R. Kristovich, B. Gleason, L. Stoecker, and R. Smith, 2012: Meteorological Causes of the Secular Variations in Observed Extreme Precipitation Events for the Conterminous United States. *Journal of Hydrometeorology*, **13**, 1131–1141, https://doi.org/10.1175/JHM-D-11-0108.1.

——, and Coauthors, 2013: Monitoring and Understanding Trends in Extreme Storms: State of Knowledge. *Bulletin of the American Meteorological Society*, **94**, 499–514, https://doi.org/10.1175/BAMS-D-11-00262.1.

Labe, Z., T. Delworth, N. Johnson, B.-T. Jong, C. McHugh, W. Cooke, and L. Jia, 2025: Large reductions in United States heat extremes found in overshoot simulations with SPEAR. *EarthArXiv*, X5TX4P, https://doi.org/10.31223/X5TX4P

Labe, Z. M., T. L. Delworth, N. C. Johnson, and W. F. Cooke, 2024: Exploring a Data-Driven Approach to Identify Regions of Change Associated With Future Climate Scenarios. *Journal of Geophysical Research: Machine Learning and Computation*, **1**, e2024JH000327, https://doi.org/10.1029/2024JH000327.

Lee, J., X. Yang, E. K. M. Chang, H. Murakami, and W. F. Cooke, 2025: Sensitivity of Northern Hemisphere Extratropical Cyclone Properties to Atmospheric Resolution in the GFDL SPEAR Model. *Journal of Climate*, **1**, https://doi.org/10.1175/JCLI-D-24-0770.1.

Lehner, F., and C. Deser, 2023: Origin, importance, and predictive limits of internal climate variability. *Environ. Res.: Climate*, **2**, 023001, https://doi.org/10.1088/2752-5295/accf30.

Li, S., L. Zhang, T. L. Delworth, W. F. Cooke, S.-Y. Song, and Q. Gu, 2024: Mitigation-driven global heat imbalance in the late 21st century. *Commun Earth Environ*, **5**, 1–11, https://doi.org/10.1038/s43247-024-01849-y.

Mankin, J. S., F. Lehner, S. Coats, and K. A. McKinnon, 2020: The Value of Initial Condition Large Ensembles to Robust Adaptation Decision-Making. *Earth's Future*, **8**, e2012EF001610, https://doi.org/10.1029/2020EF001610.

Marvel, K., and et al., 2023: *Chapter 2: Climate Trends. In: Fifth National Climate Assessment*. U.S. Global Change Research Program.

Mathesius, S., M. Hofmann, K. Caldeira, and H. J. Schellnhuber, 2015: Long-term response of oceans to CO2 removal from the atmosphere. *Nature Clim Change*, **5**, 1107–1113, https://doi.org/10.1038/nclimate2729.

McHugh, Colleen. E., T. L. Delworth, W. Cooke, and L. Jia, 2023: Using Large Ensembles to Examine Historical and Projected Changes in Record-Breaking Summertime Temperatures Over the Contiguous United States. *Earth's Future*, **11**, e2023EF003954, https://doi.org/10.1029/2023EF003954.

Meinshausen, M., and Coauthors, 2020: The shared socio-economic pathway (SSP) greenhouse gas concentrations and their extensions to 2500. *Geoscientific Model Development*, **13**, 3571–3605, https://doi.org/10.5194/gmd-13-3571-2020.

——, J. Lewis, C. McGlade, J. Gütschow, Z. Nicholls, R. Burdon, L. Cozzi, and B. Hackmann, 2022: Realization of Paris Agreement pledges may limit warming just below 2 °C. *Nature*, **604**, 304–309, https://doi.org/10.1038/s41586-022-04553-z.

Melnikova, I., and Coauthors, 2021: Carbon Cycle Response to Temperature Overshoot Beyond 2°C: An Analysis of CMIP6 Models. *Earth's Future*, **9**, e2020EF001967, https://doi.org/10.1029/2020EF001967.

Melnikova, I., and Coauthors, 2022: Impact of bioenergy crop expansion on climate–carbon cycle feedbacks in overshoot scenarios. *Earth System Dynamics*, **13**, 779–794, https://doi.org/10.5194/esd-13-779-2022.

——, P. Ciais, O. Boucher, and K. Tanaka, 2023: Assessing carbon cycle projections from complex and simple models under SSP scenarios. *Climatic Change*, **176**, 168, https://doi.org/10.1007/s10584-023-03639-5.

Mengel, M., A. Nauels, J. Rogelj, and C.-F. Schleussner, 2018: Committed sea-level rise under the Paris Agreement and the legacy of delayed mitigation action. *Nat Commun*, **9**, 601, https://doi.org/10.1038/s41467-018-02985-8.

Min, S.-K., X. Zhang, F. W. Zwiers, and G. C. Hegerl, 2011: Human contribution to more-intense precipitation extremes. *Nature*, **470**, 378–381, https://doi.org/10.1038/nature09763.

Mondal, S. K., S.-I. An, S.-K. Min, S.-K. Kim, J. Shin, S. Paik, N. Im, and C. Liu, 2023: Hysteresis and irreversibility of global extreme precipitation to anthropogenic CO2 emission. *Weather and Climate Extremes*, **40**, 100561, https://doi.org/10.1016/j.wace.2023.100561.

Murakami, H., and Coauthors, 2015: Simulation and Prediction of Category 4 and 5 Hurricanes in the High-Resolution GFDL HiFLOR Coupled Climate Model. *Journal of Climate*, **28**, 9058–9079, https://doi.org/10.1175/JCLI-D-15-0216.1.

Nazarian, R. H., J. V. Vizzard, C. P. Agostino, and N. J. Lutsko, 2022: Projected Changes in Future Extreme Precipitation over the Northeast United States in the NA-CORDEX Ensemble. *Journal of Applied Meteorology and Climatology*, **61**, 1649–1668, https://doi.org/10.1175/JAMC-D-22-0008.1.

Ning, L., E. E. Riddle, and R. S. Bradley, 2015: Projected Changes in Climate Extremes over the Northeastern United States. *Journal of Climate*, **28**, 3289–3310, https://doi.org/10.1175/JCLI-D-14-00150.1.

O'Gorman, P. A., 2015: Precipitation Extremes Under Climate Change. *Curr Clim Change Rep*, **1**, 49–59, https://doi.org/10.1007/s40641-015-0009-3.

O'Gorman, P. A., and T. Schneider, 2009: The physical basis for increases in precipitation extremes in simulations of 21st-century climate change. *Proceedings of the National Academy of Sciences*, **106**, 14773–14777, https://doi.org/10.1073/pnas.0907610106.

Olafsdottir, H. K., H. Rootzén, and D. Bolin, 2021: Extreme Rainfall Events in the Northeastern United States Become More Frequent with Rising Temperatures, but Their Intensity Distribution Remains Stable. *Journal of Climate*, **34**, 8863–8877, https://doi.org/10.1175/JCLI-D-20-0938.1.

O'Neill, B. C., and Coauthors, 2016: The Scenario Model Intercomparison Project (ScenarioMIP) for CMIP6. *Geoscientific Model Development*, **9**, 3461–3482, https://doi.org/10.5194/gmd-9-3461-2016.

Palter, J. B., T. L. Frölicher, D. Paynter, and J. G. John, 2018: Climate, ocean circulation, and sea level changes under stabilization and overshoot pathways to 1.5 K warming. *Earth System Dynamics*, **9**, 817–828, https://doi.org/10.5194/esd-9-817-2018.

Peters, G. P., 2024: Is limiting the temperature increase to 1.5°C still possible? *Dialogues on Climate Change*, **1**, 63–66, https://doi.org/10.1177/29768659241293218.

Pfleiderer, P., C.-F. Schleussner, and J. Sillmann, 2024: Limited reversal of regional climate signals in overshoot scenarios. *Environ. Res.: Climate*, **3**, 015005, https://doi.org/10.1088/2752-5295/ad1c45.

Picard, C. J., J. M. Winter, C. Cockburn, J. Hanrahan, N. G. Teale, P. J. Clemins, and B. Beckage, 2023: Twenty-first century increases in total and extreme precipitation across the Northeastern USA. *Climatic Change*, **176**, 72, https://doi.org/10.1007/s10584-023-03545-w.

Pielke, R., M. G. Burgess, and J. Ritchie, 2022: Plausible 2005–2050 emissions scenarios project between 2 °C and 3 °C of warming by 2100. *Environ. Res. Lett.*, **17**, 024027, https://doi.org/10.1088/1748-9326/ac4ebf.

Prütz, R., J. Strefler, J. Rogelj, and S. Fuss, 2023: Understanding the carbon dioxide removal range in 1.5 °C compatible and high overshoot pathways. *Environ. Res. Commun.*, **5**, 041005, https://doi.org/10.1088/2515-7620/accdba.

Raftery, A. E., A. Zimmer, D. M. W. Frierson, R. Startz, and P. Liu, 2017: Less than 2 °C warming by 2100 unlikely. *Nature Clim Change*, **7**, 637–641, https://doi.org/10.1038/nclimate3352.

Reisinger, A., and Coauthors, 2025: Overshoot: A Conceptual Review of Exceeding and Returning to Global Warming of 1.5°C.

Riahi, K., and Coauthors, 2017: The Shared Socioeconomic Pathways and their energy, land use, and greenhouse gas emissions implications: An overview. *Global Environmental Change*, **42**, 153–168, https://doi.org/10.1016/j.gloenvcha.2016.05.009.

Rogelj, J., and Coauthors, 2018: Scenarios towards limiting global mean temperature increase below 1.5 °C. *Nature Clim Change*, **8**, 325–332, https://doi.org/10.1038/s41558-018-0091-3.

Roldán-Gómez, P. J., P. De Luca, R. Bernardello, and M. G. Donat, 2025: Regional irreversibility of mean and extreme surface air temperature and precipitation in CMIP6 overshoot scenarios associated with interhemispheric temperature asymmetries. *Earth System Dynamics*, **16**, 1–27, https://doi.org/10.5194/esd-16-1-2025.

Samanta, A., B. T. Anderson, S. Ganguly, Y. Knyazikhin, R. R. Nemani, and R. B. Myneni, 2010: Physical Climate Response to a Reduction of Anthropogenic Climate Forcing. *Earth Interactions*, **14**, 1–11, https://doi.org/10.1175/2010EI325.1.

Samset, B. H., J. S. Fuglestvedt, and M. T. Lund, 2020: Delayed emergence of a global temperature response after emission mitigation. *Nat Commun*, **11**, 3261, https://doi.org/10.1038/s41467-020-17001-1.

Schiemann, R., P. L. Vidale, L. C. Shaffrey, S. J. Johnson, M. J. Roberts, M.-E. Demory, M. S. Mizielinski, and J. Strachan, 2018: Mean and extreme precipitation over European river basins better simulated in a 25 km AGCM. *Hydrology and Earth System Sciences*, **22**, 3933–3950, https://doi.org/10.5194/hess-22-3933-2018.

Schleussner, C.-F., and Coauthors, 2024: Overconfidence in climate overshoot. *Nature*, **634**, 366–373, https://doi.org/10.1038/s41586-024-08020-9.

Seneviratne, S. I., and Coauthors, 2021: Weather and Climate Extreme Events in a Changing Climate. In Climate Change 2021: The Physical Science Basis. Contribution of Working Group I to the Sixth Assessment Report of the Intergovernmental Panel on Climate Change. Cambridge University Press, 1513–1766.

Solomon, S., G.-K. Plattner, R. Knutti, and P. Friedlingstein, 2009: Irreversible climate change due to carbon dioxide emissions. *Proceedings of the National Academy of Sciences*, **106**, 1704–1709, https://doi.org/10.1073/pnas.0812721106.

Stansfield, A. M., K. A. Reed, C. M. Zarzycki, P. A. Ullrich, and D. R. Chavas, 2020: Assessing Tropical Cyclones' Contribution to Precipitation over the Eastern United States and Sensitivity to the Variable-Resolution Domain Extent. *Journal of Hydrometeorology*, **21**, 1425–1445, https://doi.org/10.1175/JHM-D-19-0240.1.

Steinert, N. J., J. Schwinger, R. Chadwick, J.-S. Kug, and H. Lee, 2025: Irreversible Land Water Availability Changes From a Potential ITCZ Shift During Temperature Overshoot. *Earth's Future*, **13**, e2024EF005787, https://doi.org/10.1029/2024EF005787.

Sun, Q., X. Zhang, F. Zwiers, S. Westra, and L. V. Alexander, 2021: A Global, Continental, and Regional Analysis of Changes in Extreme Precipitation. *Journal of Climate*, **34**, 243–258, https://doi.org/10.1175/JCLI-D-19-0892.1.

Tebaldi, C., and P. Friedlingstein, 2013: Delayed detection of climate mitigation benefits due to climate inertia and variability. *Proceedings of the National Academy of Sciences*, **110**, 17229–17234, https://doi.org/10.1073/pnas.1300005110.

——, and Coauthors, 2021: Climate model projections from the Scenario Model Intercomparison Project (ScenarioMIP) of CMIP6. *Earth System Dynamics*, **12**, 253–293, https://doi.org/10.5194/esd-12-253-2021.

Thackeray, C. W., A. Hall, J. Norris, and D. Chen, 2022: Constraining the increased frequency of global precipitation extremes under warming. *Nat. Clim. Chang.*, **12**, 441–448, https://doi.org/10.1038/s41558-022-01329-1.

Thibeault, J. M., and A. Seth, 2014: Changing climate extremes in the Northeast United States: observations and projections from CMIP5. *Climatic Change*, **127**, 273–287, https://doi.org/10.1007/s10584-014-1257-2.

Tokarska, K. B., K. Zickfeld, and J. Rogelj, 2019: Path Independence of Carbon Budgets When Meeting a Stringent Global Mean Temperature Target After an Overshoot. *Earth's Future*, **7**, 1283–1295, https://doi.org/10.1029/2019EF001312.

UNFCC, 2015: *FCCC/CP/2015/L.9/Rev.1: Adoption of the Paris Agreement*.

Van der Wiel, K., and Coauthors, 2016: The Resolution Dependence of Contiguous U.S. Precipitation Extremes in Response to CO2 Forcing. *Journal of Climate*, **29**, 7991–8012, https://doi.org/10.1175/JCLI-D-16-0307.1.

Walton, J., and C. Huntingford, 2024: Little evidence of hysteresis in regional precipitation, when indexed by global temperature rise and fall in an overshoot climate simulation. *Environ. Res. Lett.*, **19**, 084028, https://doi.org/10.1088/1748-9326/ad60de.

Wehner, M. F., R. L. Smith, G. Bala, and P. Duffy, 2010: The effect of horizontal resolution on simulation of very extreme US precipitation events in a global atmosphere model. *Clim Dyn*, **34**, 241–247, https://doi.org/10.1007/s00382-009-0656-y.

——, and Coauthors, 2014: The effect of horizontal resolution on simulation quality in the Community Atmospheric Model, CAM5.1. *Journal of Advances in Modeling Earth Systems*, **6**, 980–997, https://doi.org/10.1002/2013MS000276.

Westra, S., L. V. Alexander, and F. W. Zwiers, 2013: Global Increasing Trends in Annual Maximum Daily Precipitation. *Journal of Climate*, **26**, 3904–3918, https://doi.org/10.1175/JCLI-D-12-00502.1.

Whitehead, J. C., and Coauthors, 2023: *Chapter 21. Northeast. In: Fifth National Climate Assessment*. U.S. Global Change Research Program.

Zappa, G., P. Ceppi, and T. G. Shepherd, 2020: Time-evolving sea-surface warming patterns modulate the climate change response of subtropical precipitation over land. *Proceedings of the National Academy of Sciences*, **117**, 4539–4545, https://doi.org/10.1073/pnas.1911015117.

Zhang, X., H. Wan, F. W. Zwiers, G. C. Hegerl, and S.-K. Min, 2013: Attributing intensification of precipitation extremes to human influence. *Geophysical Research Letters*, **40**, 5252–5257, https://doi.org/10.1002/grl.51010.

Zhao, M., and Coauthors, 2018: The GFDL Global Atmosphere and Land Model AM4.0/LM4.0: 1. Simulation Characteristics With Prescribed SSTs. *Journal of Advances in Modeling Earth Systems*, **10**, 691–734, https://doi.org/10.1002/2017MS001208.

Zickfeld, K., and Coauthors, 2013: Long-Term Climate Change Commitment and Reversibility: An EMIC Intercomparison. *Journal of Climate*, **26**, 5782–5809, https://doi.org/10.1175/JCLI-D-12-00584.1.

——, A. H. MacDougall, and H. D. Matthews, 2016: On the proportionality between global temperature change and cumulative CO2 emissions during periods of net negative CO2 emissions. *Environ. Res. Lett.*, **11**, 055006, https://doi.org/10.1088/1748-9326/11/5/055006.

——, D. Azevedo, S. Mathesius, and H. D. Matthews, 2021: Asymmetry in the climate–carbon cycle response to positive and negative CO2 emissions. *Nat. Clim. Chang.*, **11**, 613–617, https://doi.org/10.1038/s41558-021-01061-2.

Supplementary Information

"Reversal of extreme precipitation trends over the Northeast US in response to aggressive climate mitigation in GFDL SPEAR"

Bor-Ting Jong[1,2,3,*], Zachary M. Labe[4,5], Thomas L. Delworth[5], and Willam F. Cooke[5]

[1] Department of Earth Sciences, Vrije Universiteit Amsterdam, Amsterdam, The Netherlands

[2] Institute for Environmental Studies, Vrije Universiteit Amsterdam, Amsterdam, The Netherlands

[3] Atmospheric and Oceanic Sciences Program, Princeton University, Princeton, NJ, USA

[4] Climate Central, Inc., Princeton, NJ, USA

[5] NOAA/OAR/Geophysical Fluid Dynamical Laboratory, Princeton, NJ, USA

*Corresponding author: Bor-Ting Jong (b.jong@vu.nl)

Contents in this file: Table S1 & Figures S1-S4

This EarthArXiv original "preprint" has been submitted to Environmental Research Letters and has not been peer-reviewed or edited.

Table S1. Summary of the two models (SPEAR_HI and SPEAR_MED) and their associated climate scenario simulations used in this study.

	Radiative forcing scenarios	Year	Horizontal resolutions	Ensemble members
SPEAR_HI	SSP5-8.5	2015-2100	• 0.25° ×0.25° in atmosphere/land • 1° ×1° in ocean	10
	SSP5-3.4OS	2015-2100		6
	CMIP6 Historical Forcing	1951-2014		10
	Preindustrial Control*	1-1000		-
SPEAR_MED	SSP5-8.5	2015-2100	• 0.5° ×0.5° in atmosphere/land • 1° ×1° in ocean	30
	SSP5-3.4OS	2015-2100		30
	CMIP6 Historical Forcing	1951-2014		30
	Preindustrial Control*	1-3000		-

* The control simulations use atmospheric composition fixed at levels representative of the year 1850.

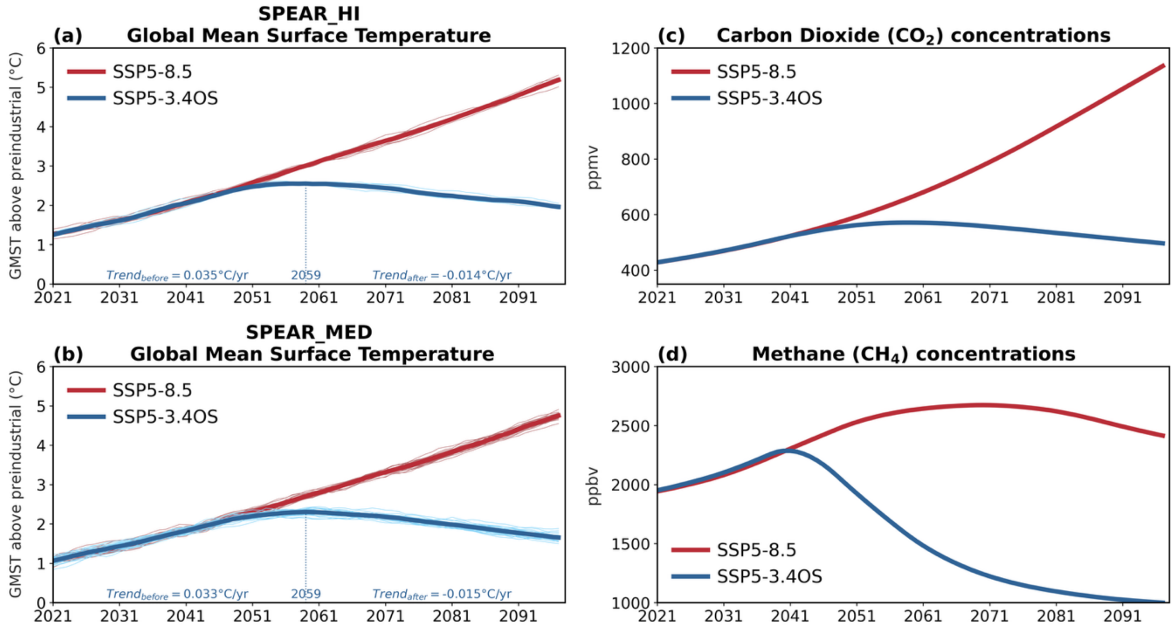

Figure S1. (a), (b) Time-series of annual global mean surface temperature (GMST) anomalies from 2021 to 2100 under the SSP5-8.5 (red) and SSP5-3.4OS (blue) scenarios from **(a)** SPEAR_HI and **(b)** SPEAR_MED. GMST anomalies are relative to the preindustrial mean GMST. Thick lines represent the ensemble mean, and thin lines show individual ensemble members. The year in which GMST peaks under SSP5-3.4OS (2059 in both SPEAR_HI and SPEAR_MED) is marked in each panel. Linear least squares trends of GMST before and after the peak warming are also noted. The time-series are smoothed with a 7-year running mean centered on each year to remove the interannual variability. **(c)** Time-series of annual mean atmospheric carbon dioxide (CO_2) concentrations (parts per million by volume) from 2021 to 2100 in SSP5-8.5 (red) and SSP5-3.4OS (blue) in the SPEAR models. **(d)** as in (c), but for methane (CH_4) concentrations (parts per billion by volume).

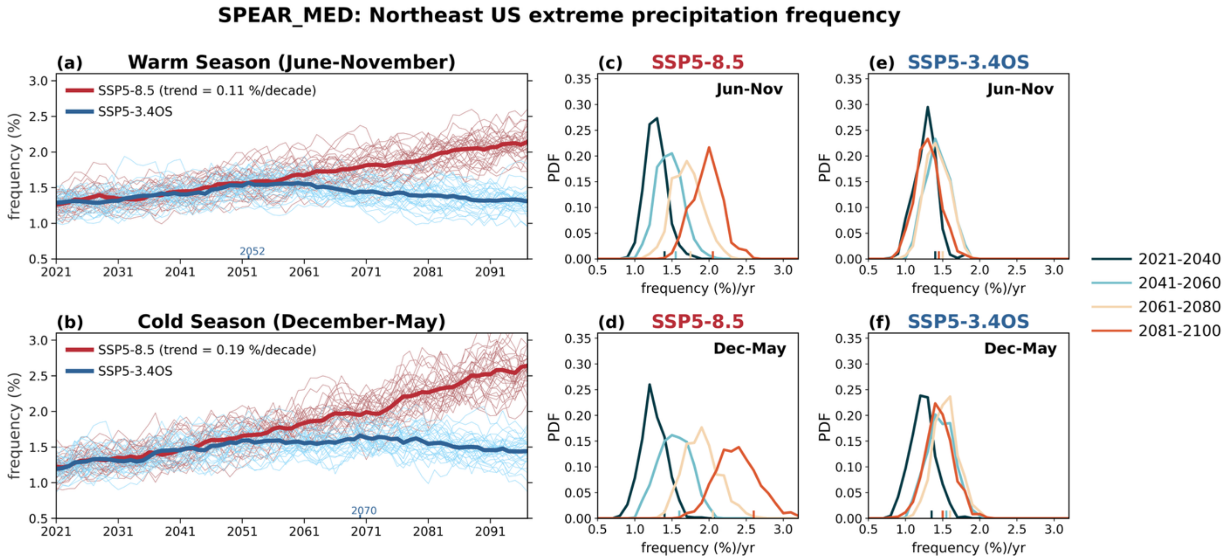

Figure S2. Changes in the frequency of extreme precipitation over the Northeast US from 2021 to 2100 in SPEAR_MED. **(a), (b)** Time-series of extreme precipitation frequency under the SSP5-8.5 (red) and SSP5-3.4OS (blue) scenarios in the **(a)** warm season (June-November) and **(b)** cold season (December-May). Thick lines represent the ensemble mean, and thin lines show individual ensemble members. All time-series are smoothed with a 7-year running mean centered on each year to remove the interannual variability. The year in which frequency peaks under SSP5-3.4OS (2052 for the warm season and 2070 for the cold season) is marked in each panel. **(c)-(f)** Changes in the distribution of extreme precipitation frequency under **(left)** SSP5-8.5 and (**right)** SSP5-3.4OS in the (**top)** warm season and **(bottom)** cold season. Each colored line presents the probability density function (PDF) of extreme precipitation frequency per year in a 20-year period. Median values of each PDF are labelled by tick marks along the x-axis.

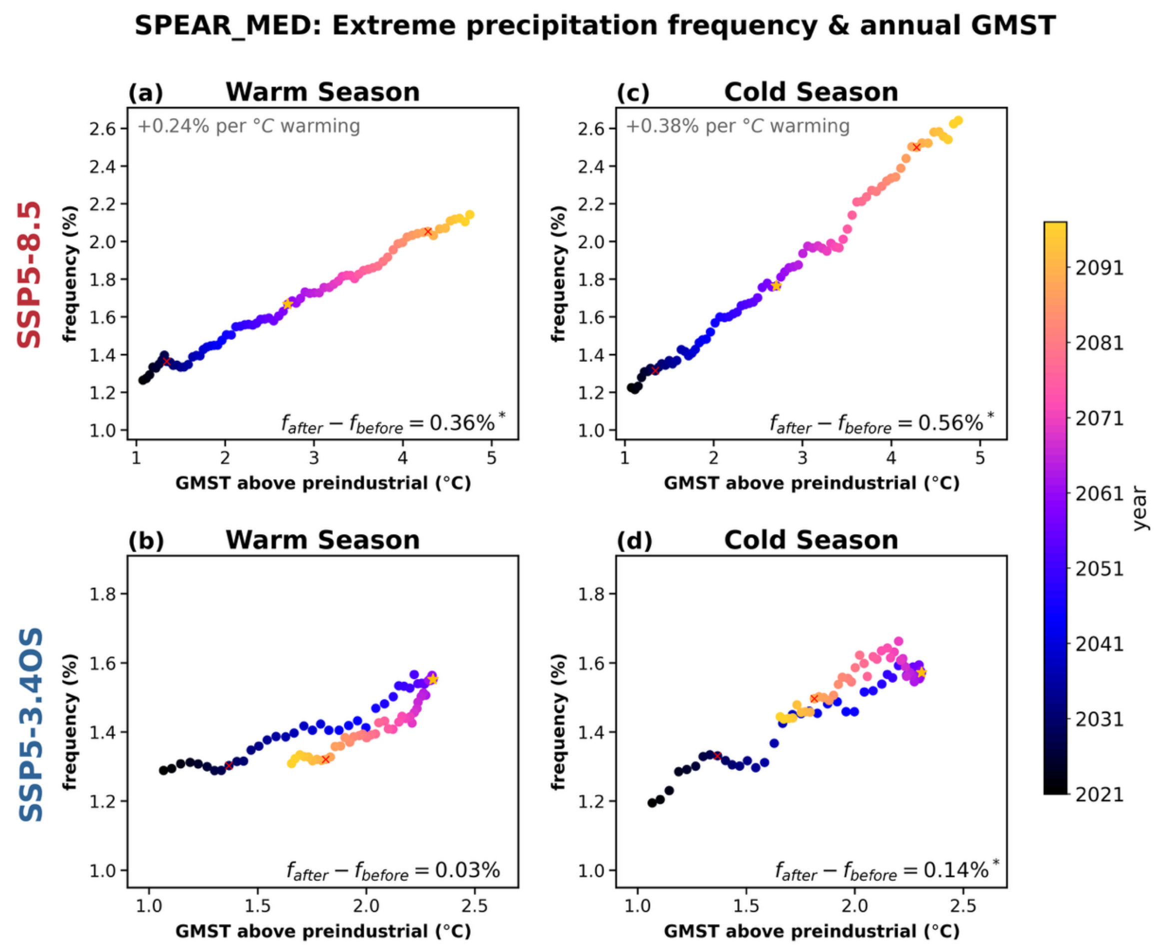

Figure S3. Changes in extreme precipitation frequency as a function of GMST anomaly in SPEAR_MED in **(top)** SSP5-8.5 and **(bottom)** SSP5-3.4OS, for the **(left)** warm season and **(right)** cold season. Each dot represents the ensemble mean from SPEAR_MED for a given year, with color indicating the year. Both GMST and frequency are smoothed with a 7-year running mean centered on each year. The difference in the 30-year average frequency before and after the peak warming year under SSP5-3.4OS is shown in the lower-right corner of each panel. Asterisks denote statistically significant differences between the two periods at the 95% confidence level. The point corresponding to the peak warming year (2059) under SSP5-3.4OS is marked with a yellow star, and the red crosses indicate the years 30 years before and after the peak.

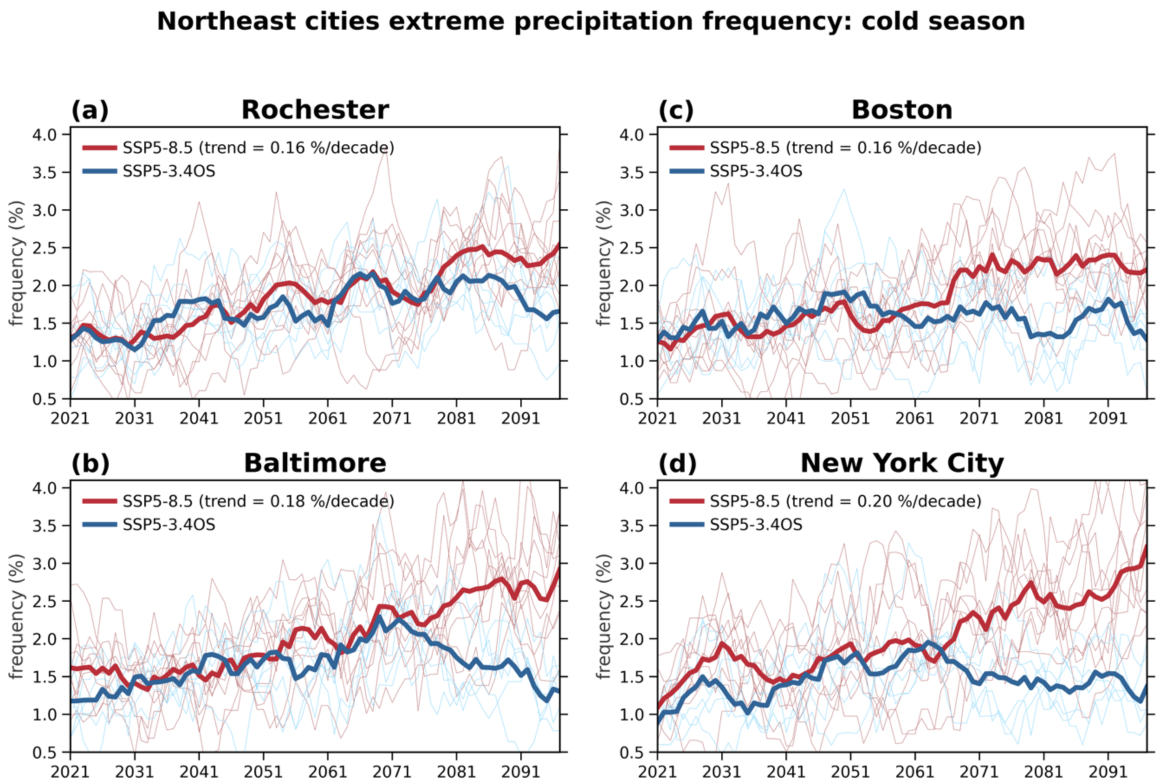

Figure S4. Time-series of extreme precipitation frequency in **(a)** Rochester, **(b)** Baltimore, **(c)** Boston, and **(d)** New York City in the cold season in SPEAR_HI. Red and blue lines are for the SSP5-8.5 and SSP5-3.4OS scenarios, respectively. Thick lines represent the ensemble mean, and thin lines show individual ensemble members. All time-series are smoothed with a 7-year running mean centered on each year.